Proceedings of the ASME 2024 Heat Transfer Summer Conference HT2024 July 15 – 17, 2024, Anaheim, CA

#### SHTC2024-131218

# A Convolution Neural Network Design for Combined Image and Sensor Data Analysis to Determine Droplet Vaporization Regime and Heat Transfer Performance

# Ursan Tchouteng Njike, Anisa Silva and Van P. Carey

Mechanical Engineering Department University of California, Berkeley, CA, USA

#### **ABSTRACT**

Combining high-speed video cameras and optimal measurement techniques with digital sensors controlled by a data acquisition system can yield a combination of experimental tools to explore boiling process thermophysics and heat transfer mechanisms. Imaging can provide qualitative and quantitative information that complements data provided by temperature, pressure, and more sensors. This paper summarizes the results of an exploration of machine learning strategies to optimally combine and analyze boiling process images and digital sensor information from experiments. We specifically sought a convolution neural network to analyze the vaporization of deposited water droplets on superheated surfaces that may have varying degrees of nucleate boiling effects. Through experimentation, we found that a hybrid parallel-series convolution/neuron neural network design worked very effectively. The network could extract the regime of droplet vaporization (conduction driven only, conduction plus nucleate boiling, or explosive boiling), the liquid morphology, and could predict the vaporization regime, the wall superheat, and mean heat transfer rate as a function of image input and operating system parameters. Using data collected from the droplet deposition experiment, this network design has been trained to predict the mean heat transfer rate with a root mean square percent error (RMSPE) of only 3.3% and 7.2% on a training and testing dataset respectively. The hybrid network developed in this research appears to be a promising strategy for analyzing experimental data for physical systems that are best investigated experimentally with a combined use of imaging and digital sensor instrumentation.

## 1. INTRODUCTION

Convolution Neural Networks (CNN) were developed in the 1980s and forms the backbone of many computer vision applications. These applications range from self-driving vehicles to medical image analysis, facial recognition and more. Recent studies of boiling heat transfer have explored ways to leverage this powerful tool to better understand boiling processes. The paper of Yang, et al. [1] discusses the use of high-speed camera visualization to examine flow boiling in microchannels. The study aims to use a CNN model to identify the flow pattern for use as a means of an accurate heat transfer mechanism prediction for applications. To achieve an optimized performance, the image was pre-processed to address issues related to unbalanced lighting and other effects that may not be relevant to the classification of pattern flow. In another similar study, Lee [2] explored strategies to optimize experimental observation and measurements of pool boiling heat transfer using computer vision techniques. The computer vision applied in that study performs bubble detection and segmentation to track bubble movements as they depart from the surface. This helps in capturing key performance parameters such as bubble density, size, and departure frequency autonomously.

When applying a CNN model to a system, a common approach is to examine simulated data of the system as an initial step. An example is the recent study by Lee et al. [3], which explored the controlled rearing of newborn chicks using deep CNN neural networks. In this study, the authors looked at simulated image data of chicks' visual observations from an agent moving within a virtual controlled-rearing chamber to compare the learning ability of a newborn chick to that of a CNN. Computer vision in medical imaging such as Magnetic Resonance Imaging (MRI) studies also makes use of simulated data to ensure the computation can understand certain features before delving into real images. Minnema, et al. [4] employed an approach of this type in their recent study that compared convolutional neural network training strategies for cone-beam CT image segmentation. This study performed image segmentation on simulated con-beam computed tomography (CBCT) to find the best way to examine the image scanned. They subsequently validated their findings on experimental data.

The work summarized here focuses on the vaporization/boiling process associated with liquid water droplet depositions on a superheated surface. In an earlier

investigation, Carey, et al. [5] analyzed features and mechanisms of droplet vaporization on superheated nanostructured surfaces and compared them to pool boiling under similar conditions. These investigators assessed regime changes by examining measured surface superheat droplet size, and surface wetting data together with high-speed videos of the droplet vaporization process in their experiments. Their highspeed videos provided visual evidence of the variation of the two-phase morphology as surface superheat, droplet size and surface wetting varied. Observed variations of the regime with superheat were summarized in Fig. 10 of that paper. Observations and data from this earlier study indicate two important points related to the study summarized here. First, the earlier study documented that for water droplet vaporization at atmospheric pressure, the mean heat transfer rate depends on surface superheat, surface wetting (contact angle), initial droplet size, the morphology of the liquid, and the presence or absence of nucleate boiling at locations on the heating surface during experiments. This indicates that the liquid morphology varies with operating conditions and properties. In general, the morphology is mainly affected by pressure and surface superheat. However, in our current study, the system pressures are fixed for all the droplet deposition experiments since they were conducted at atmospheric pressure. As depicted in Fig. 1, the operating conditions and surface parameters on the left affect heat transfer performance directly, and/or they affect morphology. The second relevant point from this earlier study is that it indicates that the boiling features of vaporization of deposited water droplets on superheated surfaces are strongly similar to those for pool boiling observed in quenching experiments under similar conditions. Droplet deposition experiments therefore can be used to explore nucleate boiling mechanisms near the onset of nucleate boiling while providing imaging access close to the surface, which allows more effective use of optical methods to obtain image information about the process.

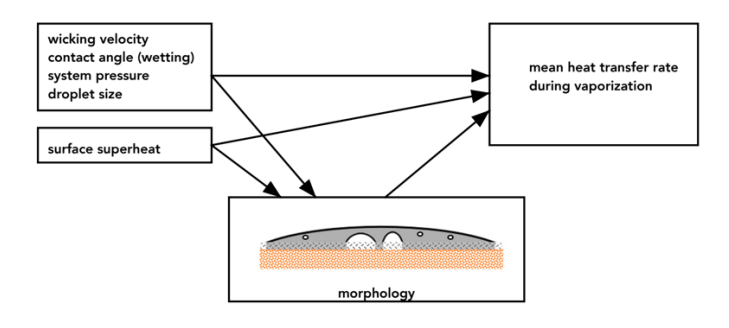


Figure 1. Study Summary

Note that the results of the earlier experiments of Carey, et al. [5] exploring droplet vaporization on superheated surfaces analyzes experimental results by converting information from video frame images to digital data. The study summarized here specifically explored an alternative approach that uses machine

learning to directly extract information from video images using a customized Convolution Neural Network (CNN).

To explore how image information can be directly used to assess liquid-vapor morphology or predict heat transfer performance, we constructed a data set containing digital data and simulated images that exhibit trends observed in the real experimental results of the earlier study of Carey, et al. [5]. As discussed above, the use of simulated images in this manner to explore the feasibility of a machine learning strategy has been commonly used in other applications, particularly for medical imaging (see, for example, the study of Minnema, et al. [4]). Here we used this approach as a first step towards evaluating a CNN-based machine learning strategy for analyzing boiling experiment results. In this preliminary work, we demonstrated the feasibility of using a specially designed CNN with skip connections to analyze a combination of digital data and morphology images to predict heat transfer performance. Using this simulated data, we also were able to optimize the design of the custom convolution neural network model. Following this initial work, we explored the use of this type of CNN model by adapting it to the flow of real droplet vaporization data that we obtained in new experiments conducted as part of this study. The details of the simulated data and the real data machine learning analysis studies are described in the following sections.

# 2. METHODS: SIMULATED DATA 2.1. Data Collection

In our simulated data study, a database was created with 138 images and their corresponding operating conditions and parameter values. The trends in this database matched the trends observed in the data from the earlier study by Carey, et al. [5]. The simulated images were created using a drawing tool called EazyDraw. The simulation exhibits specific features we may observe in a real physical system such as a change in morphology with respect to a change in its physical condition. Figure 2 depicts the different morphology observed, which are spherical cap, thin continuous line, irregular thin continuous line, and shattered regime. As shown in Fig. 1, the CNN model task is to capture the morphology features in the image data as well as the physical conditions of the system to make predictions of the mean heat transfer rate. The physical condition of the system explored has a wall superheat temperature that ranges from 0.87 K to 56.4 K above saturation temperature and a relative atmospheric pressure that ranges from 0.47 to 2.13. Both the superheat temperature and atmospheric pressures are needed to adequately make predictions of the mean heat transfer rate.

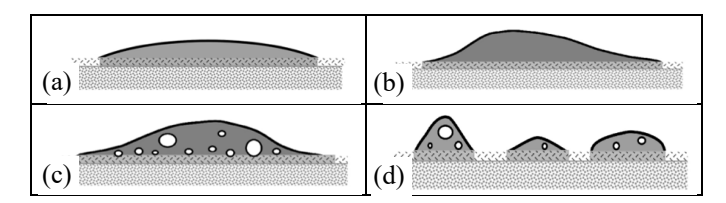


Figure 2. Simulated Images Morphology Classes: (a) Spherical Cap, (b) Thin Continuous, (c) Irregular Thin Continuous, and (d) Shattered.

In the first step of this investigation, the image data and relative atmospheric pressure were used as input data for the CNN and the wall superheat temperature was used as output data. To train the CNN model efficiently, the data needed to be preprocessed. Python, with its useful open-source libraries, was the programming language used in this paper. The input and output data were preprocessed to ensure the model interacted with data of similar ranges of values. The original images were converted to grayscale since the coloration was consistent for all images. This operation also helps to minimize the computational cost since greyscale images are represented by only one layer of numerical values as compared to color scale, which is represented by 3 layers. The image input column was converted to an image array of numerical values using the cv2 package, a package widely used for computer vision applications in Python. The images were resized to 200x50 pixels. The value of the image input array was divided by 255 since pixels in computers are encoded in values ranging from 0 - 255. This results in an input image array with values that lie between 0 and 1. The other input column consists of the relative atmospheric pressure whose median value was 1 and did not require preprocessing. On the other hand, each image had an associated morphology class label and wall superheat temperature. These were used as output values to train the CNN. The morphology class labels were converted to numerical values using one hot encoding from Keras.utils library. The superheat values were standardized by dividing them by the median superheat. In the case of this investigation, the median superheat value was 19.8 K. By performing these preprocess transformations, most of the data values were around the vicinity of 1. The entire dataset was arranged in a data frame using the Pandas package, widely used to manipulate tabular data.

Since the amount of input data was very low, there was a need to adopt a strategy to remedy this condition. Performing data augmentation is a widely adopted strategy for this kind of situation. The process consists of performing several small modifications to each image in the dataset such as a horizontal shift of the image to the right or left. This operation helps to increase the robustness ofthe CNN model. ImageDataGenerator from Keras was used in this study. The parameter of the generator includes random rotation of up to 5 degrees. It also includes horizontal shift, vertical shift, shear, and zoom of up to 10%. Random horizontal flips were allowed to be performed on the images as well. Empty spaces due to the image modification were filled using the nearest pixel value strategy. The resulting data augmented images were added to

the original 138 images totaling 3588 image data. These images with their corresponding labels were ready to be trained. The model architecture to train this data needed to be customized in such a way that it could simultaneously take the image and relative atmospheric pressure data as input. Also, the model needs to simultaneously predict the morphology class and the wall superheat temperature.

#### 2.2. Neural Network Development

For higher flexibility in building the desired convolution neural network model, the Keras functional API (Application Program Interface) was used. This API allows each layer of the network to be initialized as a function. This allows for an easy increase in complexity in the model development. The model developed here had to consider that 1 of the inputs is an array of numbers with the shape 200x50 representing the image input while the other input is a variable representing the relative atmospheric pressure. There are 2 outputs to be predicted by the model. One of the outputs requires a classification approach while the other needs a continuous variable approach such as regression. The resulting model architecture to fit this requirement is shown in Fig. 3. This architecture is divided into four regions. The first region is the input region. This is where the image and relative atmospheric pressure are captured. The second region is the convolution region. This region processes the image input and captures the features by passing the 3x3 convolution window with 32 filters across the image input with a stride of 1, or one step at a time, and a same padding type, meaning that a padding is added to the input image to ensure that the output, after the convolution process, have the same shape as the input image. A convolution layer attempts to capture patterns such as the edges of an object present in the image by passing a convolution window onto the image array one step at a time. An example of this operation is shown in Fig. 4. To add nonlinearity to the process, a Rectified Linear Unit (ReLU) activation function is applied to the output of the convolution operation. A 2x2 Max pooling layer of stride 2 and a same padding type is applied to summarize the features captured. An example of this operation is shown in Fig. 5. A same padding in max pooling allows padding to be added as needed to make up for an imperfect fit for the max pooling operation. This set of three operations is repeated once to capture more complex features of the image. The output from the two stacked sets of operation is flattened as it is moved to the fully connected region of the architecture. In this region, the flattened layer passes through a dense layer with 32 neurons. A ReLU activation function is applied to the layer to add nonlinearity. The relative atmospheric pressure is then appended to the resulting output through a concatenation layer. From this, the data is passed through a dense layer with 4 neurons and a softmax activation function to generate the morphology classification prediction. Since we are dealing with classification and regression, the regression part of the architecture has been laid out similarly. The input image is passed to a two-stacked set of convolution operations then gets

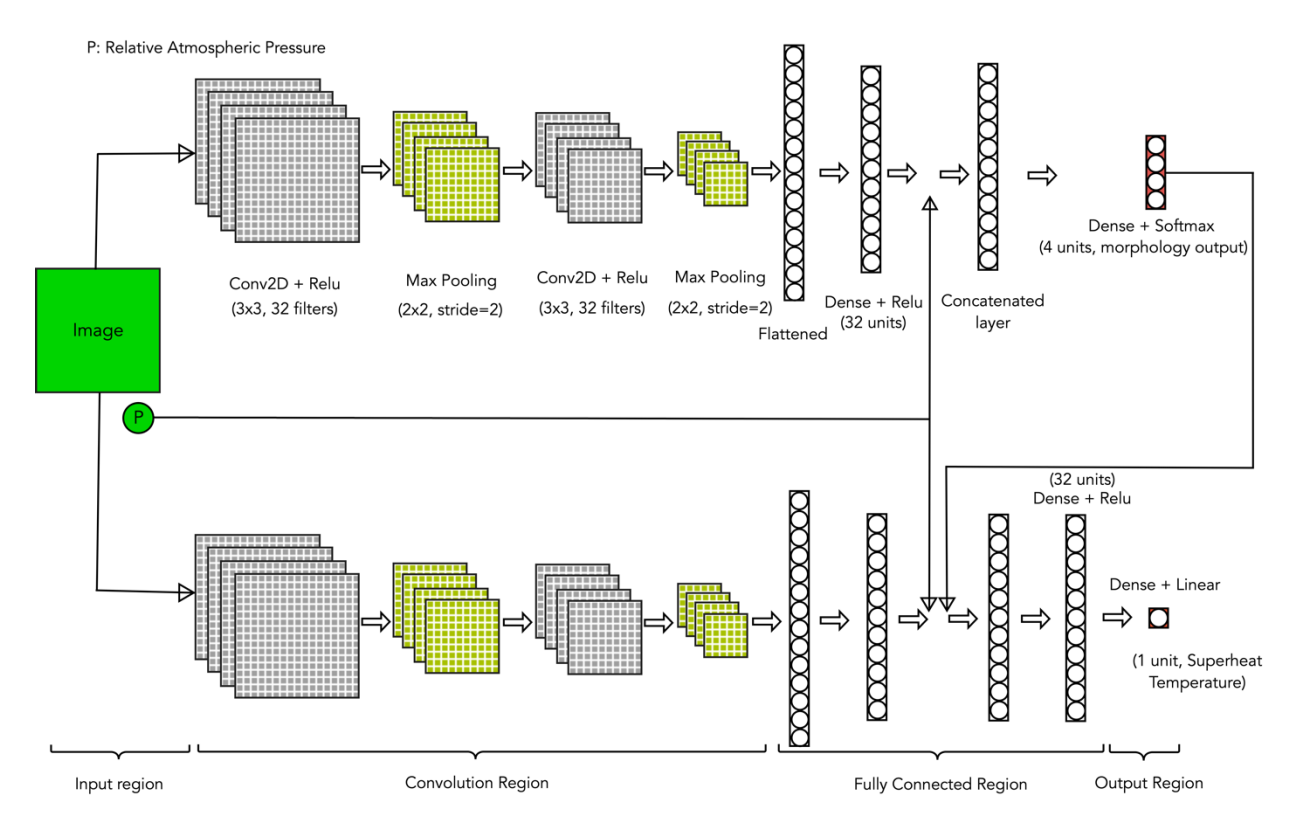


Figure 3. Convolution Neural Network Architecture for Simulated Data

flattened and is passed to a dense layer with 32 neurons and ReLU activation function. From this point, the operations differ from the classification route. The classification output and the relative atmospheric pressure inputs are appended to the result after the dense layer and ReLU activation via a concatenation layer. The concatenated layer output is passed to another dense layer with 32 neurons and a ReLU activation function. The result here is passed to a final convolution layer with one neuron and a linear activation function to predict the wall superheat temperature. With this structure, the model was trained on the 3588 images with their labels.

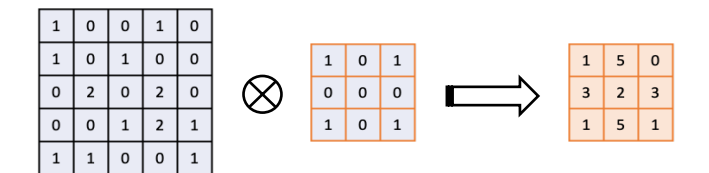


Figure 4. Convolution Operation Example

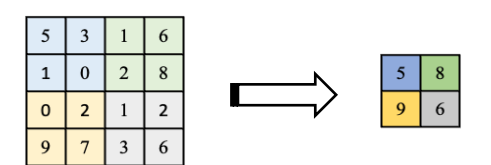


Figure 5. Max Pooling Example

#### 2.3. Results and Discussion

The model depicted in Fig. 3 fulfills all the requirements necessary to train the convolution neural network to predict the morphology class and superheat temperature. An Adam optimizer was used in the model training. Adam stands for adaptive moment estimator. This optimizer helps stochastic batch processes to converge faster to an optimal solution. its input value in this study was decreased going from 10<sup>-3</sup> to 10<sup>-6</sup> as needed to optimize the loss in the model prediction. In our case, the loss strategy used for the morphology classification was the categorical cross entropy while that for superheat prediction was the mean absolute error. Each of these losses was weighted equally in the optimization model. The training batch size was set at 32. 25% of the data was used as a validation set. The training was performed on 75% of the data. The model converged to an average loss of 0.05 on the validation set. The model was then tested on a new set of data with 100 observations generated from the simulated droplet model. Figures 6 and 7 illustrate the result obtained from the optimized convolutional neural network tested on a new set of unseen data. On the testing dataset in the simulated sample images, we observed a perfect morphology classification in all four classes of image data. Also, the wall superheat temperature prediction performed well with a root mean square percent error (RMSPE) of only 12% on a set of unseen data. This strong predictive capability suggests that the approach used in this

investigation to train the model is a promising analysis of boiling process images. This is an indication that the model has been able to successfully learn relevant patterns present in the image to make accurate classifications.

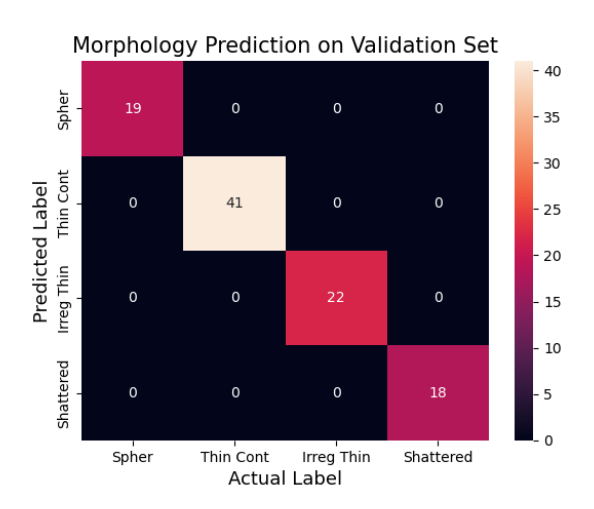


Figure 6. Morphology Classification Result on a Test Dataset for Simulated Images

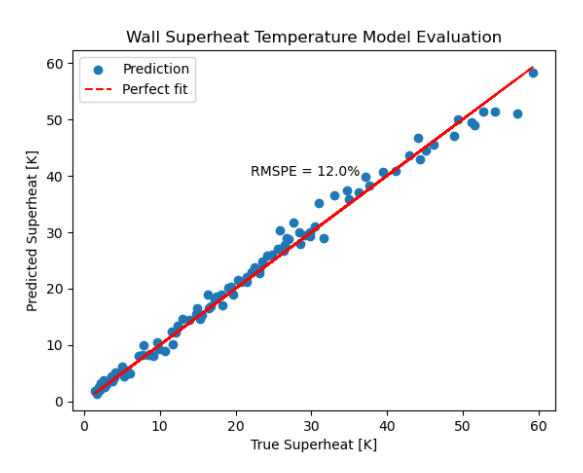


Figure 7. Superheat Prediction on a Test Dataset for Simulated Images with RMSPE of 12%

# 3. METHODS: EXPERIMENTAL DATA 3.1. Data Collection

Since the work on the simulated image yields attractive results. It was needed to perform further investigation on experimental data. The data was collected via a droplet deposition experiment. A surface that exhibits a particular contact angle  $\theta$  and wicking speed is coated on the top of a cylindrical copper rod measuring 2.5 cm in Diameter. The contact angles of water on the coated surfaces were measured using a spherical cap model. On the side of the rod, about 1 mm from the top, two holes are drilled opposite to each other for the insertion of a thermocouple for temperature measurements. This rod is placed on a hot plate with mineral wool insulation of about 1 cm thick on the sides to ensure an adiabatic process. The hot plate is adjusted to a temperature above the nucleation temperature of water. Thermocouples are inserted in the adequate holes of the cylindrical rod closer to the top, where the droplet is deposited. These thermocouple temperature readings are used to define the wall superheat temperatures. The droplet sizes are measured using a pipette at the time of deposition. A high-speed camera is placed above the rod to capture the droplet boiling process. The experiment tracks the image, superheat temperature, droplet size, and contact angle as input data. The experiment also tracks the regime classification and heat transfer rate as output data. A schematic of the droplet experiment is shown in Fig. 8. The mean heat transfer rates were calculated using Eq. (1). This equation only involves the latent heat needed to transform the droplet into steam. The energy used to raise the temperature of the droplet to saturation was ignored since it is negligible when compared to the latent heat. In this equation,  $\bar{q}$  is the mean heat transfer rate,  $\rho$  is the density of water,  $V_0$  is the initial volume of the droplet,  $h_{lv}$  is the latent heat of vaporization of water, f is the framerate of the camera, and n is the number of frames between the droplet getting in contact with the surface and its complete evaporation. The framerate of the camera used in this study was 1200 frames per second.

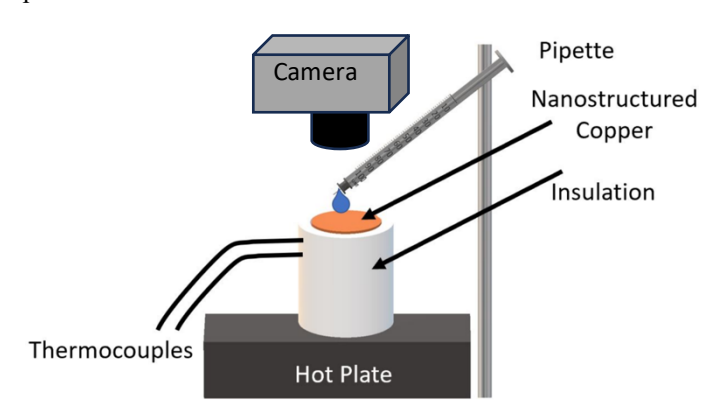


Figure 8. Droplet Deposition Experiment

$$\bar{\dot{q}} = \frac{\rho V_0 h_{lv} f}{n} \tag{1}$$

experiment. The images were selected based on their information richness, i.e. presence of bubbles or gradual shrink, as captured by the camera. A sample of the image data collected is shown in Table 1 for the different morphology considered in this study. This table shows images for different droplet sizes at distinct superheat temperatures. 428 image data were generated from this experiment. This data was split into two sets. 15% of the image data was retained as a test set to evaluate the accuracy of the model on unseen data. The remaining 85% of the image data were augmented using the same approach as discussed in the simulated image data section and this set was used as a training set. The parameter of the augmentation generator includes random rotation of up to 5 degrees. It also includes horizontal shift, vertical shift, shear, and zoom of up to 10%.

Random horizontal flips were allowed to be performed on the images as well. Empty spaces due to the image modification were filled using the nearest pixel value strategy. The purpose of the data augmentation is to help in generating a robust model by deliberately adding perturbation to the image data. The data augmentation resulted in a set of 9438 images augmented from 363 of the original images randomly chosen for model training purposes. As discussed in the simulated section, these input images as well as all the other values used in training the model were preprocessed to eliminate unwanted bias toward higher magnitude values. The images were normalized by dividing the pixel values by 255 just like in the simulated model section. This ensured that arrays representing images only have values in the range of 0 to 1. The superheat temperature, droplet size, and contact angle data are normalized by dividing by their respective median values. The regime morphology classification is converted to numerical value via one hot encoding. Since the coloration of the image does not carry a physical interpretation in this experiment, all the original images were converted to grayscale. This conversion significantly reduces the computational cost for training the model since it deals with only one layer array representing the image. The images are then rescaled to 100x100 pixels to further reduce computational cost. At this resolution, most of the important features of the image are still preserved. Table 2 shows the range of data values captured during the experiments.

Conduction	<b>Isolated Bubble</b>	Vigorous Nucleation
Size = $5 \mu L\Delta T = 5K$	Size = $5 \mu L\Delta T = 20K$	Size = $5 \mu L \Delta T = 8K$
Size = $6 \mu L\Delta T = 5K$	Size = $6 \mu L \Delta T = 20 K$	Size = $6 \mu L \Delta T = 35 K$
Size = $7 \mu L \Delta T = 5K$	Size = $7 \mu L\Delta T = 20 K$	Size = $7 \mu L\Delta T = 35K$
Size = $8 \mu L\Delta T = 5K$	Size = $8 \mu L\Delta T = 20K$	Size = $8 \mu L \Delta T = 35 K$

Variable	Range
Superheat Temperature	5 – 40 [K]
Droplet Size	$5-8 [\mu L]$
Contact Angle	4.41 - 4.88 [°]
Mean Heat Transfer Rate	5.02 – 89.3 [W]

Table 2. Range of Values Used in the Study

#### 3.2. Network Architecture

Three cases were examined to understand CNN's potential in levering image features for improved mean heat transfer rate prediction. Since the CNN architecture for the simulated data yielded promising results, an adaptation of the architecture was used for each of the cases examined. The three cases are summarized in Table 3. Case A examines the architecture on its strength with information unrelated to the appearance of the droplet. Case B examines the architecture with information unrelated to the temperature of the system. Case C examines the architecture considering both the appearance of the droplet and the temperature of the system.

Case A	Case B	Case C
Input:	Input:	Input:
- Superheat Temperature	- Image Data	- Image Data
- Initial Droplet Size	- Initial Droplet Size	- Initial Droplet Size
- Contact Angle	- Contact Angle	- Contact Angle
		- Superheat
		Temperature
Output:	Output:	Output:
- Mean Heat	- Mean Heat	- Mean Heat
Transfer Rate	Transfer Rate	Transfer Rate
	- Superheat	- Nucleation
	Temperature	Regime

Table 3. Model Cases Highlighting the Inputs and Outputs Considered.

### 3.2.1. Case A

Case A's architecture aims to produce a model that does not take any information related to the appearance of the droplet. Therefore, all paths taken by the image as well as the morphology path must be eliminated from the previous CNN architecture. This adaptation aims at establishing a benchmark for the system without image input. The goal is to see whether the wall superheat temperature, contact angle, and droplet size

Table 1. Droplet Deposition Image Data of Different Droplet Sizes for each Regime Considered.  $\Delta T$  is the wall superheat  $T_w - T_{sat}$ .

used as input can attain a better solution than one that considers an input image. Figure 9 depicts the resulting architecture due to the elimination of the image input and morphology path.

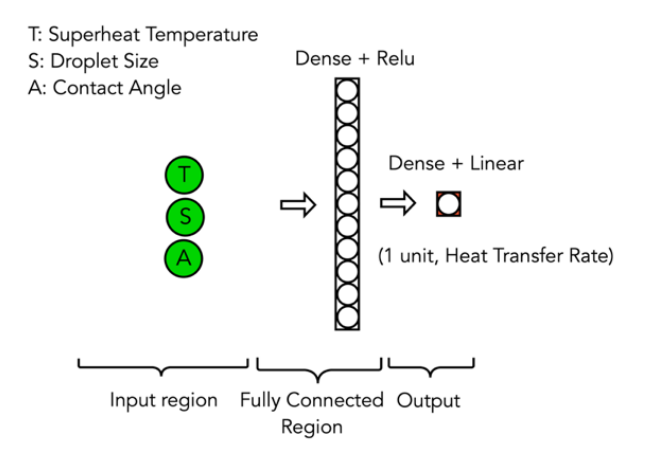


Figure 9. CNN Architecture for Case A

As shown above, eliminating the path taken by the image input results in a simple fully connected neural network with 3 numerical variables as input and one variable as output data. The 3 input data pass through a dense layer with 32 neurons that has a ReLU activation function. From this dense layer, the data moves to the final layer for output, which is another dense layer, but with a 1 neuron that has a linear activation function. This architecture has no convolution region since it does not process image information. With this architecture, the training data set described in section 3.1 was used to train a model. After training the model, we obtain the result shown in Fig. 10.

The RMSPE was evaluated on both the training and testing datasets and was found to be 13.2% and 13.6% respectively. These results demonstrate that even without information about the droplet appearance outstanding prediction can be achieved. Also, Fig. 11 shows a surface plot generated to predict the mean heat transfer rate for Case A. The contact angle for the plot was fixed at 4.65°. This plot spans the range of values for the droplet sizes and temperature values studied in this paper. It provides a full picture of the predictive model behavior throughout the droplet sizes and superheat temperature space. From the surface plot, we can observe that the droplet size has limited effect on the mean heat transfer rate at low superheat, but the effect gradually increases at higher superheat values.

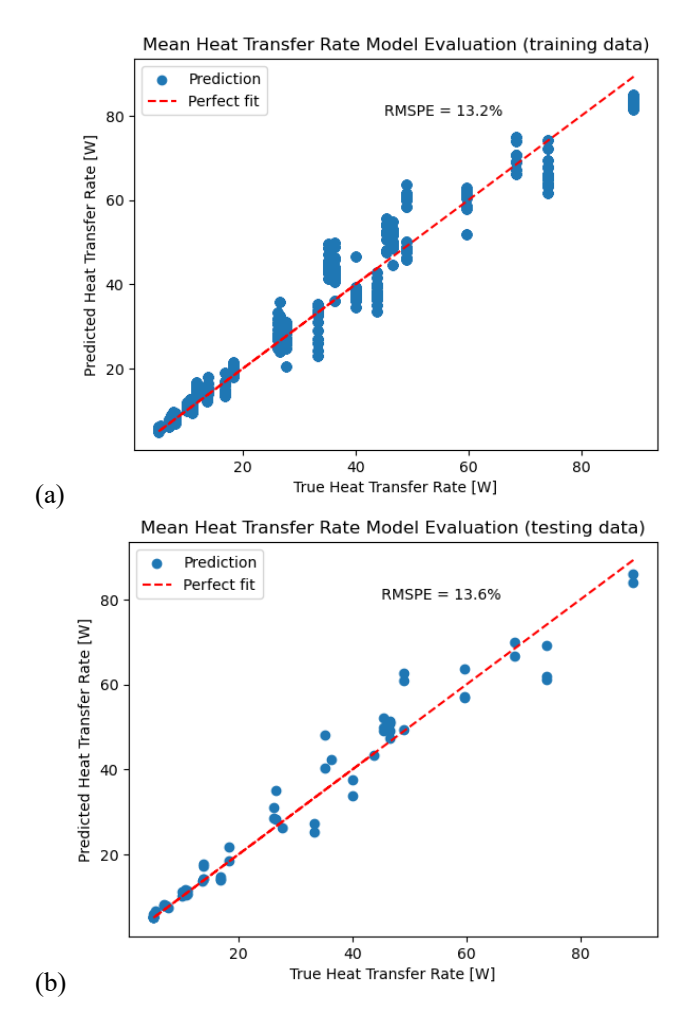


Figure 10. Mean Heat Transfer Rate Prediction results for Case A on (a) Training Dataset and (b) Testing Dataset

80 80 70 70 60 60 50 50 40 30 40 20 10 30 Superfield temperature IX 35 30 25 20 15 20 7.0 <sub>6.5 6.0</sub> 10 5 Droplet Size [µL]

Mean Heat Transfer Rate [W] ( $\Theta = 4.9^{\circ}$ )

Figure 11. Surface plot prediction of mean heat transfer rate for Case A.

#### 3.2.2 Case B

In this section, the objective is to evaluate how well a model can predict the mean heat transfer rate using an architecture similar to our preliminary study on simulated images without information about the system's temperature. The resulting architecture is depicted in Fig. 12. This architecture is configured to take a 100x100 array representation of the image data, the droplet size variable, and the contact angle variable as input, and it generates the wall superheat temperature and mean heat transfer rate as output. The image data passes through a 3x3 convolution layer with 32 filters and a same padding. From here, a ReLU activation function is applied to this convolution output to introduce nonlinearity. A 2x2 max pooling with a stride of 2 and a same padding is applied to summarize the feature captured by the convolution layer. This set of three operations is repeated one more time. As the data enters the fully connected region, the output from the convolution region is flattened. From here it passes through a dense layer with 32 neurons and a ReLU activation function. A skip connection is applied to concatenate the droplet size and contact angle input to the dense layer output. The concatenated data flows through another dense layer with 32 neurons and a ReLU activation function. From here, the data is connected to the 2 final dense layers with one neuron outputting the superheat temperature and mean heat transfer rate. The result from training a model with this architecture is shown in Fig. 13 for the mean heat transfer rate. The RMSPE was evaluated on both the training and testing datasets and was found to be 6.70% and 8.21% respectively. This result demonstrates that the model had strong predictive capability and that the model was able to capture features in the image data to generate predictions. From this result, it is suggested that the model might also accurately predict the superheat temperature. Figure 14 shows the comparison between the superheat temperature prediction against its true value both for the training and testing datasets.

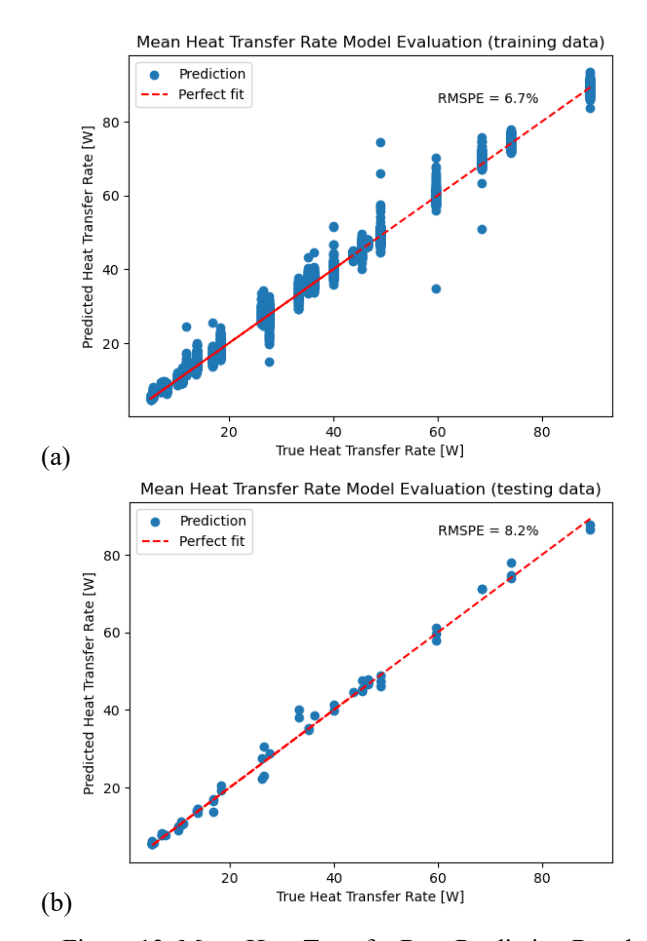


Figure 13. Mean Heat Transfer Rate Prediction Results for Case B on (a) Training Dataset and (b) Testing Dataset

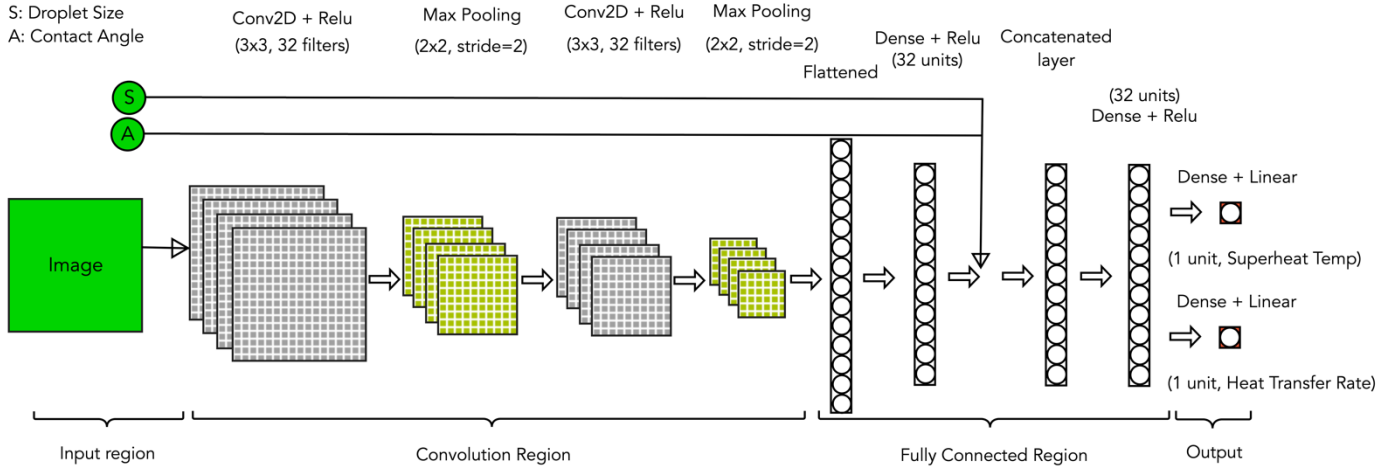


Figure 12. CNN Architecture for Case B.

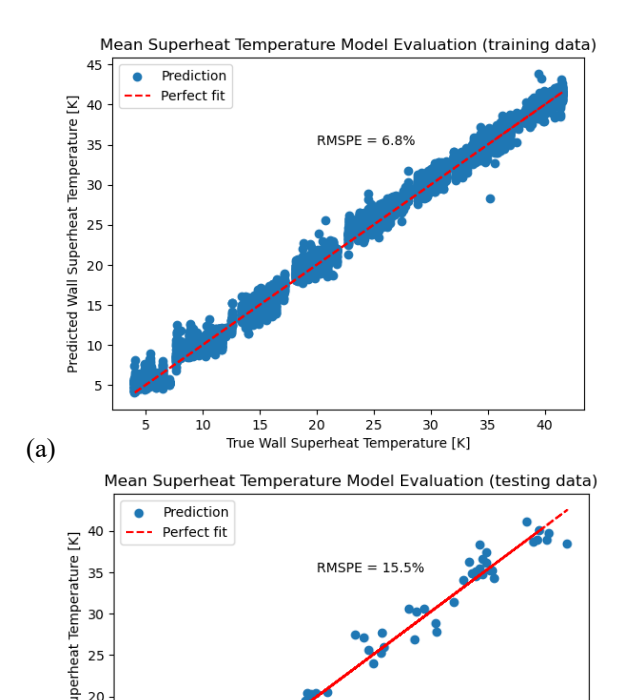


Figure 14. Superheat Temperature Prediction for Case B on (a) Training and (b) Testing Dataset

True Wall Superheat Temperature [K]

20

25

35

Predicted Wall 15

(b)

10

The model also had accurate superheat temperature predictions for both the training and testing datasets with a RMSPE of 6.82% and 15.5% respectively. One may inquire whether having both droplet appearance and temperature information as input data could generate better predictions. This question is answered by training a model on Case C's architecture.

#### 3.2.3 Case C

In this section, the focus is to explore whether combining information about the droplet appearance and the physical condition of the system can generate the strongest results among all cases. Figure 15 is the resulting architecture used in Case C. The CNN architecture here is a replica of the one used in the simulated images with few adjustments to account for desired input and output configurations.

This architecture is almost identical to the one used on the simulated image in Fig. 3. Case C's architecture differs from the architecture used on the simulated images on the input and output layer structures. The simulated model's architecture had 2 inputs, a 200x50 array representing the image and the relative pressure information, while Case C's architecture consists of 4 inputs, a 100x100 array representing the image, wall superheat temperature, droplet size, and contact angle. In addition, the output structure of the simulated images consists of a morphology with four classes and wall superheat temperature prediction while the output structure in Case C consists of a nucleation regime with three classes and a mean heat transfer rate. Every other part of the architectural structure for Case C was kept the same as the one used for the model simulation. The prediction for the model train in Case C is depicted in Fig. 16.

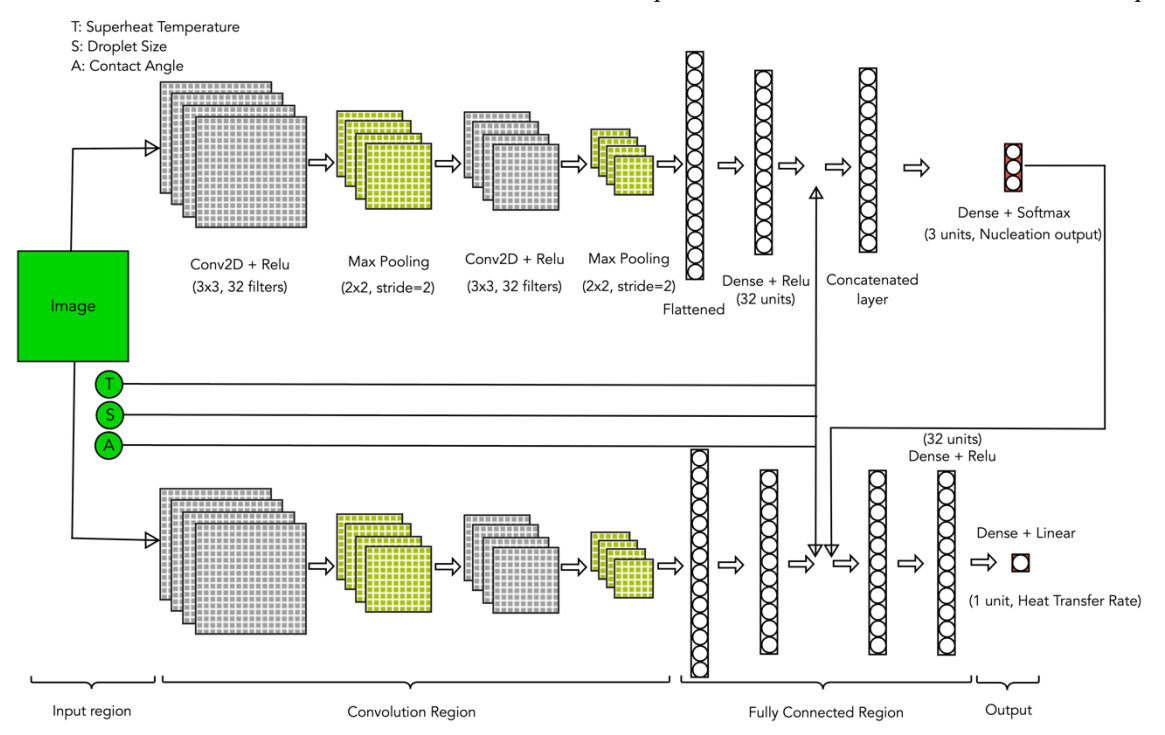


Figure 15. CNN Architecture for Case C.

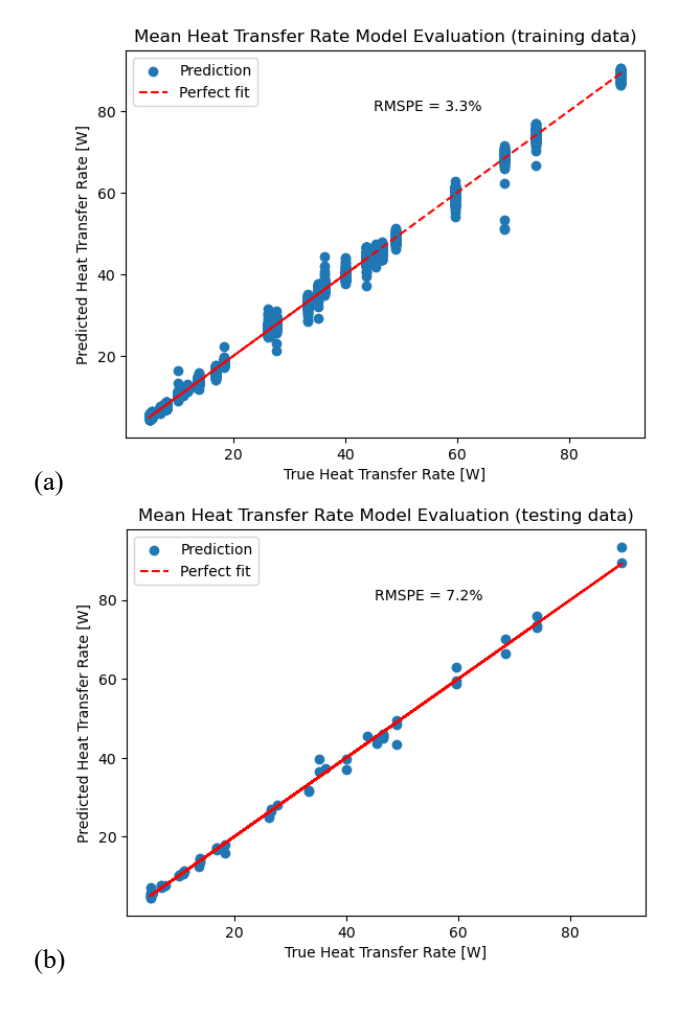


Figure 16. Mean Heat Transfer Rate Prediction results for Case C on (a) Training and (b) Testing Dataset.

The RMSPE was evaluated on both the training and testing datasets and was found to be 3.29% and 7.17% respectively. This result clearly shows an improved prediction accuracy as compared to the result obtained in Case A and Case B for predicting the mean heat transfer rate. From this result, it is believed that the model should also produce highly accurate morphology predictions. Figure 17 summarizes this prediction on both the training and testing datasets. It shows that the model predicts morphologies for all the images in the entire training dataset with 99% accuracy. The performance on the kept testing dataset misclassified 2 out of 65 images. This is an indication that the model has been able to successfully learn relevant patterns present in the image to make accurate classifications. The model for Case C was further analyzed for any distinct pattern in the data space using a stem plot of the predicted mean heat transfer rate with its corresponding regime class. From the plot shown in Figure 18, we observed trends similar to that of the surface plot for model A. Specifically, the difference in mean heat transfer along the droplet size axis seems to be more significant as the superheat temperature increases.

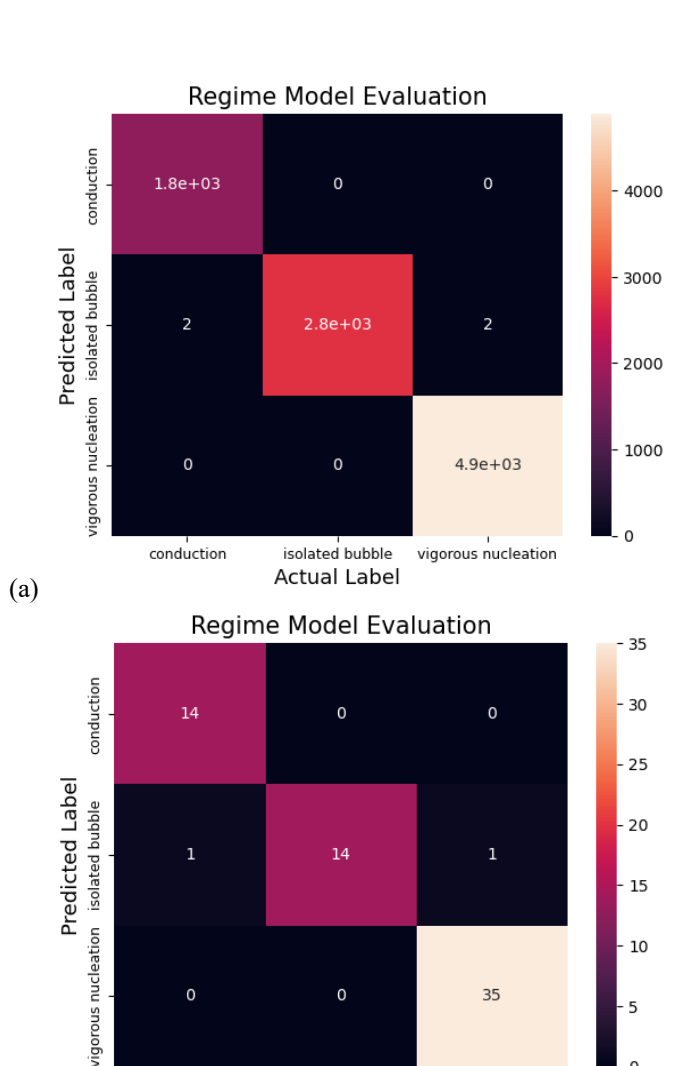


Figure 17. Nucleation Regime prediction for Case C for (a) training dataset and (b) testing dataset

conduction

(b)

0

isolated bubble

Actual Label

35

vigorous nucleation

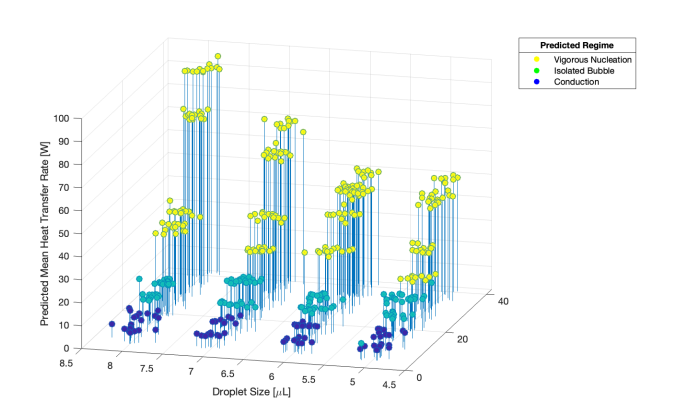


Figure 18. Predicted Mean Heat Transfer Rate using Case C Model over Input Conditions in the Entire Dataset.

# 4. EXAMINING THE USE OF IMAGE DATA AS A SUPERHEAT TEMPERATURE SENSOR FOR THE CASE A MODEL

In this section of the study, a new CNN model was trained to behave similarly to a temperature sensor. The prediction from this model was subsequently used in model A as superheat temperature input to make predictions of the mean heat transfer rate. As shown in Figure 19, the architecture of the model developed here is very similar to that of Case B explored in section 3 above. This architecture is configured to take a 100x100 array representation of the image data as input, and it generates a prediction of the wall superheat temperature as output. The image data passes through a 3x3 convolution layer with 32 filters and a same padding. From here, a ReLU activation function is applied to this convolution output to introduce non-linearity. A 2x2 max pooling with a stride of 2 and a same padding is applied to summarize the feature captured by the convolution layer. This set of three operations is repeated one more time. As the data enters the fully connected region, the output from the convolution region is flattened. From here it passes through a dense layer with 32 neurons and a ReLU activation function. The data flows through an additional dense layer with 32 neurons and a ReLU activation function. From here, the data is connected to the final dense layer with one neuron outputting the superheat temperature.

After training the CNN model using the same training dataset as the ones discussed in the previous section, we were able to get a superheat prediction with a RMSPE of 18.6% on the same testing dataset as the ones discussed in the previous section. Figure 20 depicts the observed fit to the testing dataset. These predicted superheat temperatures are then used as input temperature values to the Case A model. Figure 21 shows the observed result of the Mean Heat Transfer Rate as compared to the corresponding actual data value. This prediction has a RMSPE of 16.4%. This result implies that a CNN model can be used as a means of sensing temperature for applications such as predicting mean heat transfer rates.

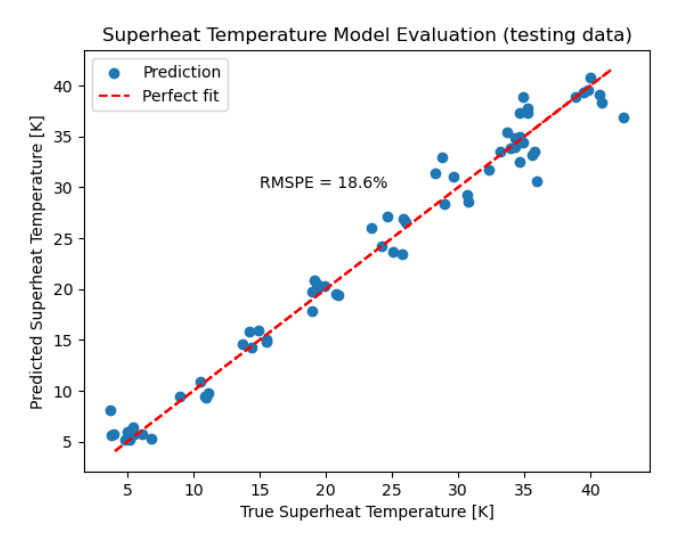


Figure 20. Superheat Temperature Prediction for CNN model as a temperature sensor

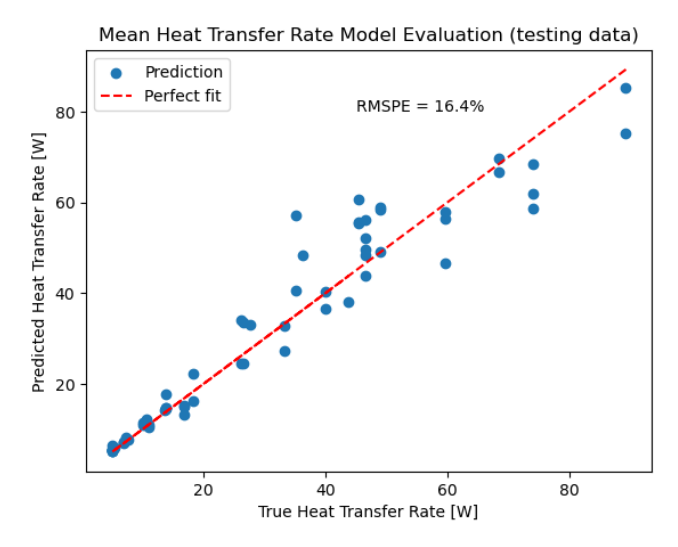


Figure 21. Mean Heat Transfer Rate using Temperature Predicted from a CNN as input to Model A

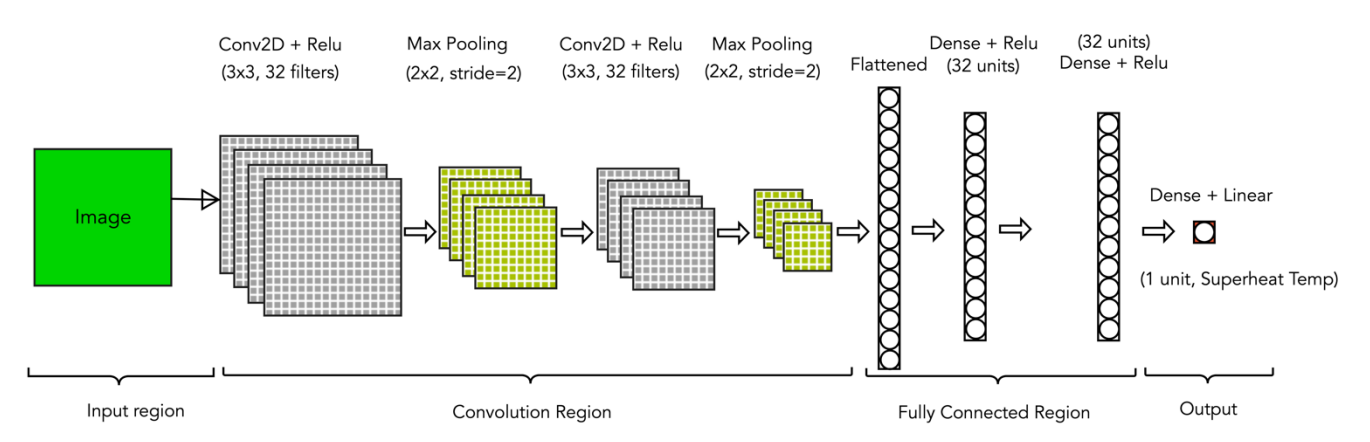


Figure 19. CNN Architecture for Predicting Superheat Temperature.

# 5. COMPARING CASE RESULTS AND CONCLUSIONS

A convolution neural network can be a powerful tool with applications in many fields. In the field of boiling heat transfer, this tool can be used to capture information hidden in the regime morphology to predict the physical properties of a system including mean heat transfer rate. Using the Python Keras functional API, it was possible to combine convolution layers and fully connected dense layers to produce a high-performing model capable of predicting the mean heat transfer rate, superheat temperature, and morphology as needed.

Four models were developed throughout this study to better understand the potential of a trained CNN model on boiling heat transfer processes. The model developed for the simulated droplet images demonstrated the capability of taking array representations of images and relative pressure values as input to predict the morphology classes and superheat temperature values. All the observations in the testing dataset were accurately classified by the model and the superheat temperature prediction had a RMSPE of 12%. Using experimental data in three distinct cases, three models were produced with high predictive capabilities. Case A's model was able to take in superheat temperature, droplet size, and contact angle values as input to predict the mean heat transfer rate with a RMSPE of 13.6% on the testing data. In Case B, the inputs were the droplet image, the droplet size, and the contact angle. These variables were used to predict the mean heat transfer rate and superheat temperatures with a RMSPE of 8.2% and 15.5% respectively on the testing data set. The model developed in Case C was the best-performing model. The model takes a droplet image, droplet volume, contact angle, and superheat temperature as input values. These values are used to predict the nucleation regime and the mean heat transfer rate. The nucleation regime had only two data misclassified out of 65 while the mean heat transfer rate was predicted with a RMSPE of 7.2%.

Our results demonstrate that the convolution neural network design, with a skip connection, developed in this study is a very effective convolution neural network (CNN) design that can be trained to predict boiling heat transfer performance with combined digital data and image information obtained in experiments. This type of modeling approach may be useful in a wide variety of boiling processes, particularly for system geometries that may complicate the liquid-vapor morphology of the system. Our results also indicate that images of the boiling two-phase morphology during deposited droplet vaporization on superheated surfaces contain information about the process that correlates with the heat transfer performance. If the image information is included in training a CNN model, the image information overlaps with wall superheat information. We found that we could train the model to predict the vaporization mean heat transfer rate with good accuracy using either the superheat or the image information. Using surface superheat information and image information combined improved model accuracy slightly in this case because the information in these two inputs is strongly (but not perfectly) correlated. The association of two-phase morphology with superheat level for pool boiling has been established empirically based on the trends and regimes in conventional boiling curves. Regimes (conduction-dominated pre-onset of nucleate boiling, fully-developed nucleate boiling, transition boiling, etc.) are generally acknowledged to correspond to specific ranges of surface superheat, each having a characteristic morphology. The study summarized here has demonstrated the correlation between surface superheat and morphology in a more direct way based on a data-science analysis. This approach may offer a means of developing a predictive model for boiling heat transfer in more complicated systems in which morphology is not simply correlated with surface superheat, and may be a useful research tool in such cases.

#### **ACKNOWLEDGEMENTS**

This work is supported by the National Science Foundation through the Graduate Research Fellowship Program and NSF CBET grant number 2228373. Funding for this research was also provided by the endowment of the A. Richard Newton Chair in Engineering at UC Berkeley

#### **REFERENCES**

[1] Yang, B., Zhu, X., Wei, B., Liu, M., Li, Y., Lv, Z., and Wang, F., 2023, "Computer Vision and Machine Learning Methods for Heat Transfer and Fluid Flow in Complex Structural Microchannels: A Review," *Energies*, 16, 1500. https://doi.org/10.3390/en16031500

[2] Lee, M., 2022, "Optimized Experimental Observation and Measurements of Pool Boiling Heat Transfer Using Computer Vision Techniques," Master's Thesis, University of California, Irvine, ProQuest Dissertations Publishing, 28971170.

[3] Lee, D., Gujarathi, P., and Wood, J. N., 2021, "Controlled-rearing studies of newborn chicks and deep neural networks", paper presented at the NeurIPS Workshop on Shared Visual Representations in Human and Machine Intelligence (SVRHM), arXiv preprint arXiv:2112.06106

[4] Minnema, J., Wolff, J., Koivisto, J., Lucka, F., Batenburg, K. J., Forouzanfar, T., and van Eijnatten, M., 2021, "Comparison of Convolutional Neural Network Training Strategies for Cone-Beam CT Image Segmentation", *Computer Methods and Programs in Biomedicine*, Vol. 207, 106192.

[5] Carey, V.P., Wemp, C.K., McClure, E.R., and Cabrera, S., 2018, "Mechanism Interaction During Droplet Evaporation on Nanostructured Hydrophilic Surfaces," paper IMECE2018-87991, *Proceedings of the ASME 2018 International Mechanical Engineering Congress and Exposition*, IMECE2018, November 9-15, 2018, Pittsburgh, PA.